Pushing the boundaries of MEG based on optically pumped magnetometers towards early human life

Pierre Corvilain[1]*, Vincent Wens[1,2], Mathieu Bourguignon[1,3], Chiara Capparini[1,4], Lauréline Fourdin[1,4], Maxime Ferez[1], Odile Feys[1,2], Xavier De Tiège[1,2] and Julie Bertels[1,4]

[1] Laboratoire de Neuroimagerie et Neuroanatomie translationnelles (LN2T), ULB Neuroscience Institute (UNI), Université libre de Bruxelles (ULB), Brussels, Belgium

[2] CUB Hôpital Erasme, Hôpital Universitaire de Bruxelles (HUB), Université libre de Bruxelles (ULB), Brussels, Belgium

[3] Laboratory of Neurophysiology and Movement Biomechanics, ULB Neuroscience Institute (UNI), Université libre de Bruxelles (ULB), Brussels, Belgium

[4] ULBabyLab – Center for Research in Cognition and Neurosciences (CRCN), ULB Neuroscience Institute (UNI), Université libre de Bruxelles (ULB), Brussels, Belgium

*e-mail: pierre.corvilain@ulb.be

Preprint: https://doi.org/10.1101/2023.10.28.564455

Classification: Biological Sciences, Neuroscience

Keywords: magnetoencephalography, optically pumped magnetometers, newborns, auditory evoked responses, steady-states responses, frequency tagging, source reconstruction

Abstract

Characterizing the early development of the human brain is critical from both fundamental and clinical perspectives. However, existing neuroimaging techniques are either not well suited to infants or have limited spatial or temporal resolution. The advent of optically pumped magnetometers (OPMs) has revolutionized magnetoencephalography (MEG) by enabling wearable and thus more naturalistic recordings while maintaining excellent sensitivity and spatiotemporal resolution. Nevertheless, its adaptation to studying neural activity in infancy poses several challenges. In this work, we present an OPM-MEG setup that successfully recorded brain responses to sounds in newborns. We exposed one-month-old infants to continuous streams of tones and observed significant evoked responses, which peaked around 250 ms poststimulus at the auditory cortex bilaterally. When tones were presented at a steady fixed pace with an oddball tone every fourth tone, significant neural responses were found both at the frequency of the standard tones (3 Hz) and of the oddball tones (0.75 Hz). The latter reflects the ability of the newborn brain to detect auditory change and synchronize to regular auditory patterns. Additional analyses support the added value of triaxial OPMs to increase the number of channels on small heads. Finally, we validated the OPM-MEG responses with those obtained from the same participants using an adult-sized cryogenic MEG. This study demonstrates the applicability of the OPM-MEG system to study early postnatal periods, a crucial step towards future OPM investigations of typical and pathological early brain development.

Introduction

During the early stages of life, the human brain undergoes major changes, with the emergence of perceptual, motor, language, social and cognitive skills. Characterizing the neurophysiological processes underlying the development of these early abilities is crucial to understanding brain maturation and brain pathologies.

However, existing brain imaging techniques are limited in investigating early brain development. While wearable systems such as electroencephalography (EEG) and near-infrared spectroscopy (NIRS) can be adapted to small heads and enable naturalistic recordings, they have limited spatial (EEG) or temporal (NIRS) resolution. Moreover, fixed systems such as functional magnetic resonance imaging (MRI) and cryogenic magnetoencephalography (MEG) have good spatial (both) and temporal (MEG) resolution but are not adapted to—and often not well tolerated by—infants. Thus, in practice, infants are often restrained or sedated when using these techniques [1].

The excellent temporal and very good spatial resolution of MEG [2] can be leveraged by having the sleeping infant rest their head on an MEG array (either using adult-size helmets in the supine position [3] or concave arrays designed to fit maternal wombs [4–7]). However, only partial head coverage can be obtained with this approach unless several recordings are performed [8]. Some efforts have been made to perform whole-head MEG scans with infants. When adult-sized cryogenic MEG systems are combined with a foam halo, the infant's head can be rigidly centered in the helmet, limiting movements [9,10], but the resulting large brain-to-sensor distance is detrimental to both the signal-to-noise ratio (SNR) and spatial resolution [11]. To address this issue, infant-sized cryogenic MEG

systems have been developed [8]; however, these systems are extremely expensive and not usable in other age ranges, so very few systems are available worldwide [12].

Optically pumped magnetometers (OPMs) are novel magnetic field sensors that offer considerable flexibility while preserving the outstanding sensitivity of cryogenic magnetometers to the subtle magnetic fields produced by neural currents [13]. In contrast to cryogenic MEG systems, in which sensors are fixed in rigid helmets, OPMs can be used to form wearable sensor arrays (OPM-MEG) that can be placed directly on the scalp, allowing more natural and flexible scanning situations [14,15]. In addition, the ensuing reduction in brain-to-sensor distance improves signal amplitude and spatial resolution [11]. Crucially, a single OPM-MEG system can be adapted to all head sizes, whereas several dedicated cryogenic MEG systems would be needed. OPM-MEG systems also consume less energy (direct electricity consumption; see Methods section) and are more affordable than cryogenic MEG systems, which is critical for their future dissemination.

The compliance of OPM-MEG has been demonstrated over a wide range of ages, starting from two years old, for both physiological [16,17] and clinical [18–20] recordings. However, the use of OPM-MEG in younger subjects poses substantial methodological challenges. First, the surface of alkali OPMs is too warm for prolonged direct contact with the skin because the rubidium inside the sensitive cell needs to be heated to approximately 150°C [15]. Therefore, due to lack of hair and skin sensitivity of newborns, efficient heat dissipation is needed to prevent discomfort and injuries. Second, multiple OPMs must be fixed on the small heads of infants to perform whole-head OPM recordings, which requires balancing ergonomics and signal quality. Recently developed triaxial OPMs increase the number of channels without impacting the ergonomics. This enables better denoising [21] and, in infant studies where spatial sampling is limited, measurements in the direction tangential to the scalp may capture neural activity missed by measurements in the radial direction [22,23].

In this work, we present a wearable whole-head OPM-MEG setup that is suitable for recordings starting from birth and we demonstrate its ability to accurately characterize early brain functions in 14 one-month-old healthy neonates. We focused on auditory stimulation, as auditory evoked brain responses occur regardless of the newborn's and behavioral state [24] and its position with respect to the speaker. We hypothesized that OPM-MEG will be able to accurately detect and localize typical auditory evoked responses as well as neural responses elicited by a fast periodic auditory oddball paradigm. We tested the added value of triaxial OPMs to increase the number of channels on small heads. Finally, we validated the OPM-MEG responses with those obtained from the same participants using an adult-sized cryogenic MEG. Overall, this work provides the foundation for future OPM-MEG neurodevelopmental studies in very young participants.

Results

System design. To balance the requirements of signal quality, adaptability, comfort and heat dissipation, we developed flexible EEG-like caps to which custom 3D-printed OPM holders that maintain the sensors 4 mm above the scalp were sewn (Fig. 1). The caps were equipped with ~27 small and lightweight alkali OPMs (Gen2/Gen3 QZFM, QuSpin Inc.), which almost entirely covered the scalp. As the newborns were meant to rest on their back, no sensors were placed in the occipital region. The setup was comfortable and light enough to be well tolerated by neonates during the whole

experiment while resting on their parent's lap or chest. This OPM-MEG setup has previously been used by our group with a 5-month-old epileptic infant to study epileptiform discharges [25]. Source reconstruction was achieved by placing the average-sized cap on a 3D printed surface of a template MRI (see Methods section and Fig. S1 in the Supplementary Material).

Fig. 1. Experimental setup. (**a**) A newborn undergoing the experiment with the OPM-MEG system. (**b**) Close-up view of the sewed-on OPM holders designed on site. The 4-mm spacing prevents direct contact between the warm OPM and the neonate scalps.

Auditory evoked responses. In a first paradigm, we presented auditory pure tones every 500–600 ms (Fig. 2a) to demonstrate that our OPM-MEG setup can reliably detect evoked responses. The grand-average evoked fields in the radial direction displayed a clear response to the stimuli (Fig. 2b). The associated topographic plot exhibited the expected dipolar pattern above the bilateral temporal regions (Fig. 2c), and its source reconstruction showed activity peaking at the auditory cortices bilaterally (Fig. 2d). This response was statistically significant from 179 ms to 359 ms poststimulus ($p < 0.0001$, maximum statistics) and its root-mean-square peaked at 261 ms. Similar analyses performed at the individual level revealed significant responses in 9 participants.

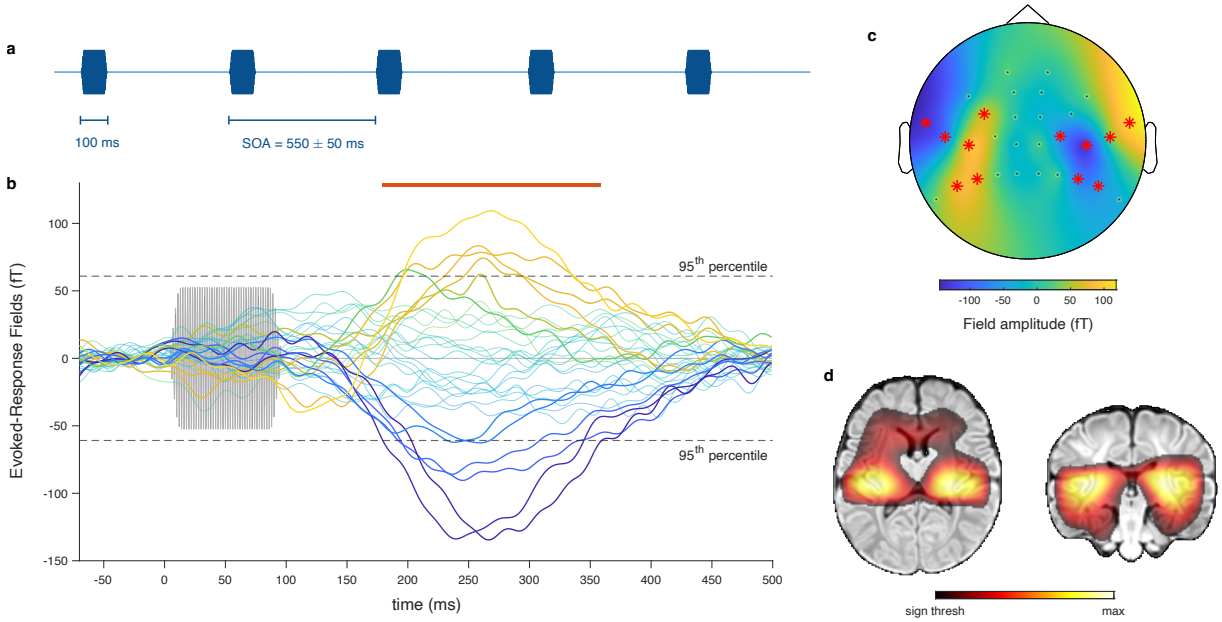

Fig. 2. Auditory evoked response paradigm. (**a**) Excerpt from the sound sequence, during which a single pure tone is presented repeatedly with a variable stimulus onset asynchrony (SOA). (**b**) Time course of the group-level evoked magnetic field measured by the OPM radial axes from -70 ms to 500 ms peristimulus. The sound stimulus is displayed in light gray (onset at 0 ms). The colors of the OPM traces match the corresponding colors on the topographic plot in panel c. Thicker traces correspond to channels showing significant responses. Periods of statistically significant responses (i.e., exceeding the 95th percentile of the surrogate distribution) are denoted with a red line above. (**c**) Topographic plot of the sensors' radial axes based on their value at the moment of highest activity (determined as the maximum of the root-mean-square across all sensors, 261 ms). Sensors showing significant responses are marked with red asterisks. (**d**) Sources activation, reconstructed from the moment of highest activity (261 ms), displayed on a template MRI of a one-month-old infant, in the neurological convention. Only statistically significant sources are displayed.

Oddball responses. In a second paradigm, we used a frequency tagging approach [26,27] to demonstrate that our OPM-MEG setup can characterize auditory change detection in newborns. For that purpose, a sequence of pure tones was presented at a steady 3 Hz rate in trains of 3 standard tones followed by one oddball tone (Fig. 3a). The SNR of the radial field power spectra, averaged across the participants, showed clear peaks at the base stimulation frequency (3 Hz), the oddball frequency (0.75 Hz), and its first harmonic (1.5 Hz) (Fig. 3b), suggesting the presence of steady-state responses at the base and oddball frequencies. Some heartbeat artifacts remained after preprocessing, leading to SNR peaks in the 2.2-2.5 Hz range, interfering with the second oddball harmonic (2.25 Hz). The topographies at 0.75 Hz, 1.5 Hz and 3 Hz showed that the corresponding SNR was localized above the temporal regions, and the source reconstruction indeed showed activity peaking at the auditory cortices bilaterally, with a right-hemisphere dominance (Fig. 3b). We performed statistical tests at those frequencies and found that SNR peaks were all significant for the group-averaged response ($p = 0.0016$, $p = 0.042$, and $p < 0.0001$, maximum statistics), and that individual responses were significant in 1, 2 and 9 participants, respectively.

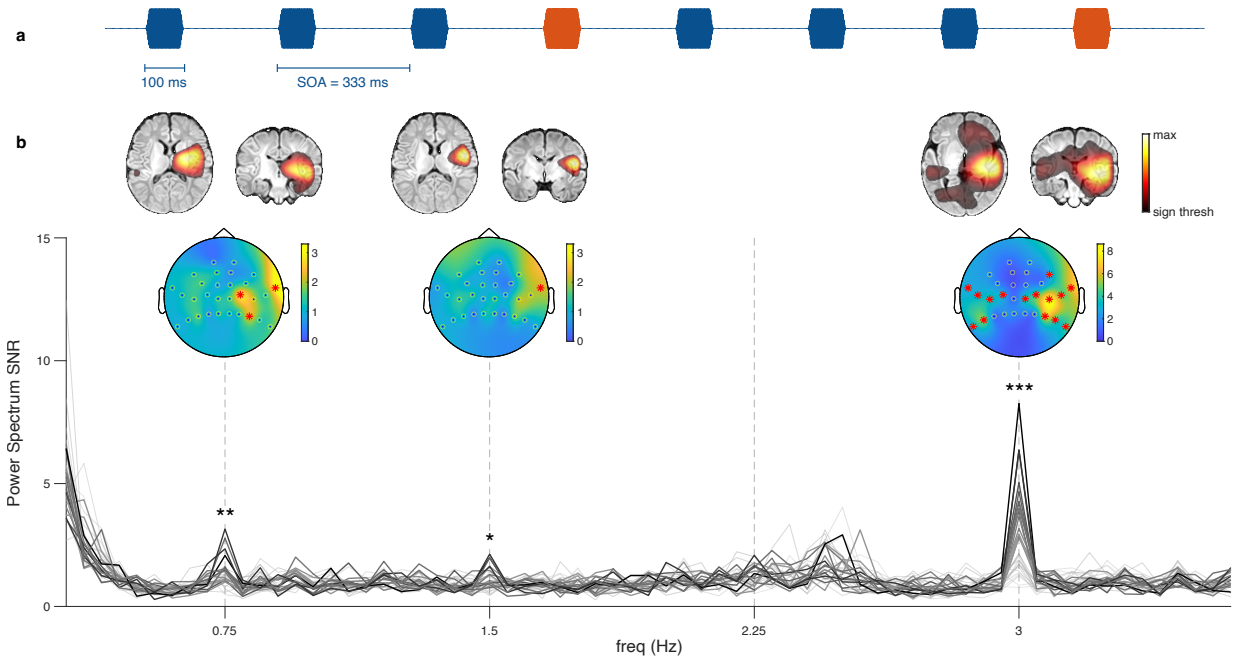

Fig. 3. Oddball paradigm. (**a**) Excerpt from the sound sequence consisting of trains of 3 base tones (blue) followed by one oddball tone (orange). The base frequency is 3 Hz, and the oddball frequency is 0.75 Hz. (**b**) Group-averaged power spectrum SNR of the OPM radial axes; the display range is 0.3-3.6 Hz. Thicker lines represent channels that were found to be significant at one of the frequencies of interest. The shade of the individual sensor curves is obtained from their SNR value at 3 Hz. Topographic plots of the SNR at the corresponding frequency are displayed above the frequencies of interest. Channels with a significant SNR are marked by red asterisks. Above are shown the reconstructed source activations at those frequencies, on a template MRI of a one-month-old infant (brain images displayed in the neurological convention). Note that this is not the source projection of the topographic plots below (see Methods section). Only statistically significant sources are displayed. Note that at the oddball frequency (0.75 Hz) a significant activity is found in both hemispheres, albeit difficult to see in the left hemisphere because of its size.

OPM tangential axes. For 10 out of the 14 participants, ~20 triaxial OPMs (Gen3 QZFM, QuSpin Inc.) were available and placed over the temporal regions. In the first paradigm, the tangential component of the fields (normed and averaged across participants) displayed a clear response to the stimuli (Fig. 4a). This response peaked at 258 ms and the associated topographic plot exhibited peak activity directly above the dipole source (Fig. 4b), i.e., between the two poles observed with the radial axes (Fig. 2c), indicating that both radial and tangential axes recorded the same activity. The response was statistically significant from 110 ms to 364 ms poststimulus onset ($p < 0.0001$, maximum statistics). Individual-level analyses revealed significant responses in 7 participants. In the second paradigm, the norm of the SNR of the OPM tangential power spectra, averaged across participants, exhibited peaks at the frequencies of interest (0.75 Hz, 1.5 Hz and 3 Hz; Fig. 4c), and all peaks were significant ($p = 0.0012$, $p = 0.0007$, $p < 0.0001$, maximum statistics). At the individual level, the responses were significant in 3, 3 and 6 participants, respectively.

We compared the tangential and radial axes responses by evaluating the individual amplitudes and SNRs of the evoked responses and the power spectrum SNRs at the base and oddball frequencies (Fig. S2 in the Supplementary Material). The power spectrum SNR at 0.75 Hz was significantly higher for the tangential axes than for the radial axes ($W = 7$, $Z = -2.09$, $p = 0.037$). No other comparison was

significant (all $p > 0.1$). The correlation between the amplitudes of the radial and tangential axes responses was very strong ($r = 0.9$, $p = 0.0003$).

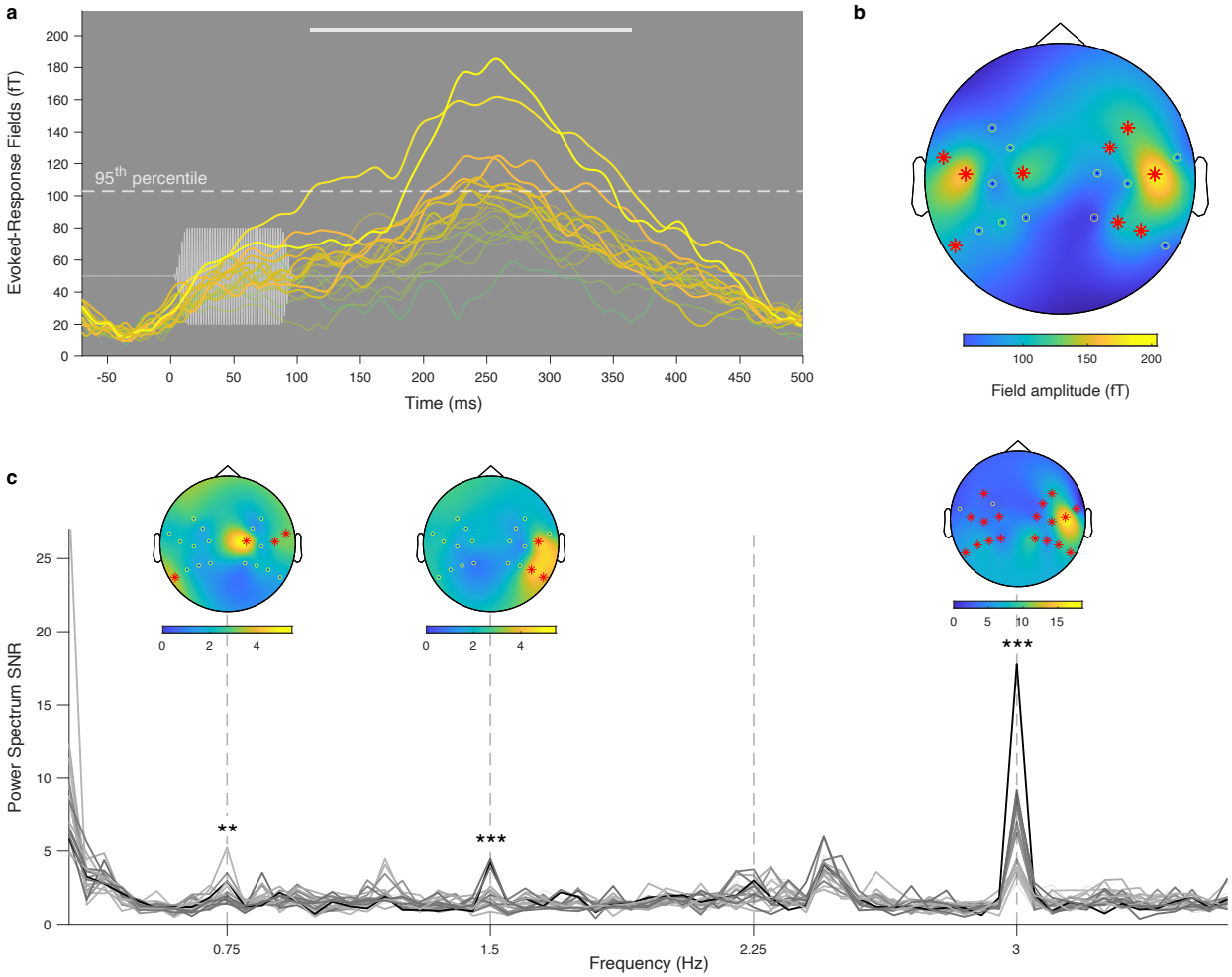

Fig. 4. Responses in the direction tangential to the scalp for the 10 participants that had triaxial OPMs placed over their temporal regions. (**a**) Norm of the tangential magnetic field responses to pure tones and (**b**) the associated topography at 258 ms. Note that the response amplitude peaks right above the source currents that can be inferred based on Fig. 2c. This is consistent with the fact that cortical sources yield magnetic fields that are mostly radial to the scalp in their neighborhood and tangential to the scalp right above the source. The rest of the plot is the same as in Fig. 2. (**c**) Norm of the tangential power spectrum SNRs in the oddball steady-state experiment. The rest of the plot is the same as in Fig. 3.

Comparison to cryogenic MEG. A subset of 7 infants were evaluated with the same paradigms in an adult-size cryogenic MEG system (Neuromag Triux, MEGIN) in the supine position, with their head laid sideways on the posterior sensor region. Our goal was to compare the recordings obtained using both modalities. The root-mean-square of the averaged auditory evoked responses peaked at 264 ms poststimulus onset with the OPM-MEG and at 282 ms with the cryogenic MEG. We compared the amplitudes and SNRs of the evoked responses and the power spectrum SNRs at the base and oddball frequencies (Fig. S3 in the Supplementary Material). The amplitude of the evoked responses was significantly higher (on average 4 times higher) with OPM-MEG than with cryogenic MEG ($t(6) = 8.05$,

p = 0.0002). This was to be expected due to the reduced brain-to-sensor distance. The SNRs of both the evoked responses and the power spectrum were not significantly different (all $p > 0.26$).

Discussion

In this work, we developed a wearable whole-head OPM-MEG setup that fits and is well tolerated by newborns. Our design, which used flexible EEG-like caps and slightly elevated OPM holders, prevented heat-related discomfort to the infants' skin. We demonstrated that this OPM-MEG system is able to acquire high-quality data by performing two auditory paradigms in a group of one-month-old healthy newborns.

In the first paradigm, the system successfully and accurately recorded the response evoked by pure tones, with similar latency as previously reported in the cryogenic MEG [3–6] and EEG [28–30] literature; in the latter, it is known as the P2 component [30] and is the only component observed at the group level in the first few months of life [31,32]. In the second paradigm, we demonstrated the possibility of using our OPM-MEG system to perform frequency tagging paradigms with newborns, which have been shown to be very fruitful with young participants [27,33]. While frequency tagging paradigms related to the one applied in this study were carried out with EEG in adults [34] and infants [35–37], steady-state responses have not yet been studied in infants with MEG, nor with tone frequency changes. The power spectrum SNR exhibited significant peaks at the base frequency, at the oddball frequency and at its first harmonic. The last two are a frequency tagging analog of the auditory mismatch negativity (MMN), reflecting automatic change detection [38]. In the frequency tagging approach, these peaks can also reveal rhythm perception and, more generally extraction of structural patterns [35–37], as the trains of stimuli are presented periodically. It is worth noting that observing an SNR peak in the spectrum at 0.75 Hz is a nontrivial feat of our system, as the OPM signal is known to be very noisy at such low frequencies due to movement and ambient field drifts [14]. Dealing with such low-frequency noise has rarely been performed [39].

Performing sources reconstruction, we were able to localize the sources of scalp magnetic fields within the infant brain at bilateral auditory cortices, as expected. The reconstructed sources had a higher intensity in the right hemisphere for the oddball responses, echoing previous observations with EEG in 2-month-old infants [40]. These results were obtained using a template MRI and an approximate estimation of sensor position and orientation. The fact that this nonetheless led to an accurate source reconstruction is a manifestation of the substantial advantage of the MEG signal not being distorted by the head tissues, compared to the EEG signal. In particular for this population, the EEG signal is distorted due to sutures and fontanels [41], and individual head models are necessary. Considering the difficulty of obtaining structural MRI in infants [42,43], which largely impacts the recruitment of participants, the proposed approach demonstrates the key added value of OPM-MEG to perform source reconstruction based on a template MRI in this population. The advent of automatic OPM localization on the subjects' scalp using the OPMs internal coils will improve the accuracy of source reconstruction.

Additionally, we showed that the neural activity is also accurately recorded by the OPMs in the direction tangential to the scalp, meaning that triaxial OPMs are a great way to increase the channel count without impacting the size and weight of the device. Although in our setup the activities

captured in the radial and tangential directions were similar, as seen from the high correlation between the response amplitudes, they turned out to be better suited to reveal significant responses in the frequency tagging paradigm. In scenarios with even smaller head sizes, such as preterm neonates, the risk of missing activity with the radial axes alone becomes higher, and having tangential axes increases the chances that all the relevant activity is captured.

Lastly, we validated our results with an adult-size cryogenic MEG. The latencies of the responses were concordant, and the amplitudes significantly higher for the OPM-MEG, as the sensors are closer to the scalp in our setup. Nevertheless, we found similar SNRs for the two MEG types, as the noise level of the OPM signal is higher. This originates in movements creating high-amplitude artefacts, due to the sensors being displaced in a nonzero magnetic field. This issue can be tempered by keeping the ambient field as low as possible, which requires strong magnetic shielding and the use of field-nulling coils, as applied in our study. Further improvements in interference suppression techniques [44,45] will likely increase the SNR of OPM data, which may ultimately exceed that of cryogenic MEG data.

Still, with a similar SNR, OPM-MEG permits whole-scalp recordings in infants without the need to build an expensive dedicated system; it is also much less energy-intensive than cryogenic MEG. Importantly, in our setup, data can be acquired in a setting that is naturalistic and appropriate for newborns, with the baby resting comfortably on their parent's lap. These advantages are likely unachievable with one-size-fits-most rigid helmets used in previous OPM studies [16]. Moreover, for this population, the large variability in head shapes and sizes would mean having to design many different rigid helmets. Our OPM-MEG setup offers the flexibility and applicability to newborns of wearable systems such as EEG, whilst providing the high spatial precision of MEG. In addition, our setup can be easily adapted to older participants (see [18,19] for studies in school-aged children), making it an MEG system that is applicable across the whole lifespan.

In conclusion, the present study reports an innovative wearable MEG system that allows for more naturalistic recordings in neonates. This research paves the way for further early neurodevelopmental investigations using OPM-MEG, which will benefit from the increased naturalness, signal amplitude and spatial resolution from the on-scalp sensors. This may ultimately provide a wealth of unprecedented information on brain functional maturation from the very early stages of life.

Materials and Methods

Participants. Fourteen neonates (7 females) participated in this study; their ages ranged between 29 and 36 days (mean: 32.6 days)**.** The inclusion criteria were as follows: gestational age >36 weeks, APGAR scores >7 at 5 and 10 minutes after birth, uncomplicated pregnancy, no known developmental delay, and normal hearing at birth (cf. otoacoustic emissions). For each paradigm, we had to reject the data of one participant (a different one in each dataset) due to technical issues. The parents gave informed consent prior to testing and received monetary compensation for their participation. The CUB Hôpital Erasme Ethics Committee approved the experimental protocol (P2021/141/B406202100081). The methods were carried out in accordance with the approved guidelines and regulations.

System design and data acquisition. To build a wearable OPM-MEG system that was suitable for newborns, we used flexible and slightly stretchy caps (EasyCap, sizes: 36, 38 and 40 cm of head

circumference), onto which we sewed OPM holders that we designed and 3D-printed with acrylonitrile butadiene styrene (ABS) on site. As a result, the interior of the cap was fabric, and the cap was comfortable to wear. The holders were set so that a gap of 4 mm was left between the scalp and the OPM (Fig. 1b), which is crucial to dissipate the heat generated by the rubidium-based OPMs and prevent hurting the sensitive skin of newborns. Indeed, the rubidium inside the sensitive cell needs to be heated to approximately 150°C to work in the spin exchange relaxation-free regime [46], making the OPM surface relatively hot. Notably, helium-based OPMs do not heat [47]; however, to date, He-OPMs are too heavy and bulky [23] to be placed on a newborn scalp, as opposed to the OPMs used in this study (size: 1.2 x 1.7 x 2.6 cm^3, weight: 4.5–4.7 g). In addition, we attached aerogel foam to the bottom of the OPMs to further isolate the scalp. The caps were equipped with 19 to 30 (mean: 27) biaxial or triaxial OPMs (Gen2/Gen3 QZFM, QuSpin Inc.), depending on the cap size and OPM availability. The 15 to 24 triaxial sensors (mean: 20, available for 10 participants) were placed in priority over the temporal areas to increase sensitivity to auditory responses [11,21]. When wearing the cap, the newborns could rest on the laps of one of their parents, seated inside a magnetically shielded room (Compact MuRoom, MSL Ltd). The room was degaussed and wall coils (MuCoils, Cerca Magnetics) were used—available for 10 participants—in order to further reduce the remanent magnetic fields below 1 nT within a 40-cm wide cubic region of interest containing the newborn's head. This was achieved by mapping, before the acquisition, the remanent static magnetic field in that cube using the offset-corrected field-zero values of ~20 triaxial OPMs positioned in that region using a custom-made all-wood structure. The magnetic profiles of the coils were determined at those positions by sending voltages in step pulses and measuring the magnetic responses with the OPMs. The latter were then inverted to null the magnetic field measured in the previous step. Data were recorded at a sampling frequency of 1200 Hz using a 16-bit digital acquisition (DAQ) system (National Instruments) controlled by a custom-made Python program. Audio stimuli were recorded simultaneously with the DAQ. If needed, the infants used a nonmagnetic pacifier. Live video was available during the whole experiment to monitor and address any problems that may have occurred. ***Direct energy consumption***. The OPMs (QuSpin Inc.) have a total direct power consumption of 5 W per sensor [48] and can be switched off when not in use. A high-density array of 128 OPMs (384 channels) used for 7 hours in one day would thus consume 4.4 kWh of electricity. For comparison, the 306-channel cryogenic MEG TRIUX neo (MEGIN) system has a minimum power consumption of 4.2 kW [49] and cannot be switched off. It therefore consumes a minimum of 100.8 kWh of electricity in one day. Taking the helium recycler [50] and the type of current used into account, the daily consumption ranges between 110 and 190 kWh. We report here only the direct energy consumption, as no life cycle analysis of both MEG types has been performed. The corresponding carbon dioxide emissions will depend on the carbon intensity of the local electricity production. However, to have an idea, one can look at the CO2-equivalent emitted assuming the mean carbon intensity of electricity production across the world, i.e., 438 gCO2e/kWh in 2022 [51]. In that scenario, the use of OPM-MEG would emit 0.7 tCO2e/year for 128 OPMs used 7 hours every single day, while possessing a cryogenic MEG would emit 17.6-30.4 tCO2e/year, regardless of its utilization.

Auditory stimuli. Both auditory paradigms consisted of 5-minute sequences of pure tones, each lasting 100 ms including 15 ms of fade-in and fade-out, presented at 65 dB using a flat MEG-compatible speaker (Panphonics). We presented each type of sequence more than once—when possible—to increase the amount of data (total number of sequences presented: 2-5, mean: 3) in a randomized order. ***Evoked response paradigm.*** In each sequence, a single pure tone with a frequency of either

500 Hz or 750 Hz (depending on the sequence) was presented with a stimulus onset asynchrony (SOA) randomly varying between 500 and 600 ms (Fig. 2a). ***Oddball paradigm.*** Pure tones were presented at a steady 3 Hz rate in trains of 3 base tones followed by one oddball tone, leading to an oddball frequency of 0.75 Hz (Fig. 3a); this paradigm was inspired by [34]. The base (oddball) tone frequency was either 500 or 750 Hz (750 or 500 Hz), depending on the sequence. For both paradigms, the sequences with different tone frequencies were treated identically for the analysis.

Data analysis. ***Preprocessing*****.** Recording periods containing large movement artifacts were first identified by visual inspection and marked as artifact time windows. Heartbeat artifacts from the newborn and the parent were then removed with an independent component analysis (ICA) [52] using the FastICA algorithm [53], which was applied to the non-artifacted part of the recordings, bandpass filtered between 1-40 Hz. Time windows affected by remaining artifacts were identified by visual examination of the other independent components by sliding through 5-second windows. ***Evoked response paradigm****.* Data in the artifact periods were replaced by linear interpolation, bandpass filtered between 1-40 Hz, and notch filtered at the frequencies at which the power spectrum displayed noise peaks, within the 13-40 Hz range. Artifact periods were extended by 1.5 s in both directions. A robust z-score rejection (channel per channel, threshold value of 5, data amplitude smoothed with a 1 s square window beforehand) was performed to identify samples affected by remaining artifacts. At this stage, the amount of data identified as artifacted was 32 % on average (standard deviation of 14 %). The first three principal components of the artifact-free data were projected out [18]. The resulting data were decomposed into epochs from -70 to 500 ms around the start of each sound presentation, and epochs that intersected artifact periods were rejected. The remaining epochs were baseline corrected, with a baseline spanning the 70 ms prestimulus period. The epochs were averaged for each participant (individual-level evoked response). The norm of the response along the tangential direction was taken. Finally, the evoked responses were averaged across all participants (group-level). ***Oddball paradigm*****.** The amount of data identified as artifacted was 22 % on average (standard deviation of 12 %). The data were bandpass filtered between 0.2-40 Hz (to maintain access to the oddball frequency), and notch filtered at the frequencies at which the power spectrum displayed noise peaks, within the 13-40 Hz range. The first three principal components estimated from the artifact-free data were projected out. The ranges of the newborn's and parent's heart rates were computed based on the components identified in the ICA preprocessing, and further components containing heartbeat artifacts were removed if, in those heart frequency ranges, their power spectrum SNR (computed as explained below) exceeded 7.5. The resulting data were decomposed into artifact-free, 20-s epochs, starting when an oddball sound was presented to preserve the stimulus-related temporal structure across epochs. The complex-valued Fourier coefficients of the data in each epoch were computed using the fast Fourier transform algorithm and averaged across epochs. The power spectrum was obtained as the squared magnitude of the resulting Fourier coefficients. Then, the SNR was computed for each frequency bin as the ratio of the power at that frequency to the mean power across the two 0.1-0.4 Hz frequency intervals around the considered frequency. The tangential SNR was computed as the norm of the SNRs in the 2 tangential directions. Group-level SNRs were obtained by averaging across participants. ***Cryogenic MEG***. Data were first denoised using signal space separation (MaxFilter, MEGIN) without movement compensation, as the head position was not tracked. Only the magnetometer data were retained, and all the other steps were the same as those for processing the OPM-MEG data, except that the three first principal components were not removed. ***Topographies*****.** Topographic plots were generated using Fieldtrip [54] and group averages were performed on the

basis of a 2D layout that most closely matched the sensor positions for all the different cap sizes used.

***Sources reconstruction*.** In the absence of MRIs of the individual participants, sources were reconstructed within a template MRI of a one-month-old infant, sourced from the Brain Connectome Project (BCP) [55]. To register the OPMs positions and orientations on this template, the head surface of the smallest available Montreal Neurological Institute (MNI) template [56] was used, as the BCP image is devoid of skin information. This head surface was rescaled to match the head circumference of our group average and centered on the BCP MRI brain volume. It was then 3D printed, the flexible cap mounted on it and populated with OPMs. The positions and orientations of the OPMs, together with the surface of the 3D printed face, were recorded using a 3D scanner (Einscan H2). Co-registration with the MRI was performed using Blender with a co-registration add-on [57], see figure S1. The forward model was computed using the one-layer Boundary Element Method of the MNE software [58]. The inner skull surface used in this model was obtained from the adult MNI inner skull surface, shrunk until it fitted snugly to the one-month-old BCP brain volume, as the latter could not be segmented. Using the Minimum-Norm Estimates inverse solution, with power bias correction [59], sources activations were reconstructed for the peak activity of the group averaged evoked response. For the oddball paradigm, sources cannot be reconstructed from group-averaged SNR as this quantity is not linear in the magnetic field. Instead, they were reconstructed per subject for the Fourier coefficients at the frequencies of interest. The power spectra and their SNRs were then computed, and the group-average was taken. For all source reconstructions, only the radial axes were taken into account.

Statistics. Maximum statistics tests were performed on the evoked and steady-state responses at both the individual and group levels, hence providing full control of the familywise error rate. The iterative *step-down method* [60] was used, i.e., data that were found to be significant in one iteration were masked off the maximum statistics test in the next iteration until no more significant data were found. The statistical significance level was set to $p < 0.05$. Null distributions were constructed from 10,000 samples of surrogate data built according to the null hypothesis that they contain no response to the stimuli. For the evoked responses in the time domain, the sign of each epoch was randomly flipped (permutation test), and for the frequency tagging analysis, the phases of Fourier coefficients were randomly changed. In both cases, the same changes were applied to all OPM channels to preserve their spatial distribution. To compare the different modalities (radial versus tangential axes, n = 10, and OPM versus cryogenic MEG, n = 7), we performed two-tailed paired sample *t*-tests, unless Shapiro–Wilk tests indicated that the distributions deviated from normality, in which case two-tailed Wilcoxon signed-rank tests were performed. For these tests, the amplitudes of the evoked responses were computed as the highest value across the channels at the point where the root-mean-square of all channels peaked. The SNR for these evoked responses was computed as the ratio between the amplitude and the standard deviation of the corresponding channel time-series during the baseline (70 ms prestimulus period). Finally, the individual power spectrum SNRs for the steady-state responses were taken as the highest power spectrum SNR value at each of the frequencies of interest.

References

1. Copeland A, Silver E, Korja R, Lehtola SJ, Merisaari H, Saukko E, et al. Infant and Child MRI: A Review of Scanning Procedures. Front Neurosci. 2021 Jul 12;15:666020.

2. Baillet S. Magnetoencephalography for brain electrophysiology and imaging. Nat Neurosci. 2017 Feb 23;20(3):327–39.

3. Huotilainen M, Kujala A, Hotakainen M, Shestakova A, Kushnerenko E, Parkkonen L, et al. Auditory magnetic responses of healthy newborns. Neuroreport. 2003 Oct 6;14(14):1871–5.

4. Lengle JM, Chen M, Wakai RT. Improved neuromagnetic detection of fetal and neonatal auditory evoked responses. Clin Neurophysiol Off J Int Fed Clin Neurophysiol. 2001 May;112(5):785–92.

5. Holst M, Eswaran H, Lowery C, Murphy P, Norton J, Preissl H. Development of auditory evoked fields in human fetuses and newborns: a longitudinal MEG study. Clin Neurophysiol Off J Int Fed Clin Neurophysiol. 2005 Aug;116(8):1949–55.

6. Draganova R, Eswaran H, Murphy P, Lowery C, Preissl H. Serial magnetoencephalographic study of fetal and newborn auditory discriminative evoked responses. Early Hum Dev. 2007 Mar;83(3):199–207.

7. Muenssinger J, Matuz T, Schleger F, Kiefer-Schmidt I, Goelz R, Wacker-Gussmann A, et al. Auditory habituation in the fetus and neonate: an fMEG study. Dev Sci. 2013 Mar;16(2):287–95.

8. Chen YH, Saby J, Kuschner E, Gaetz W, Edgar JC, Roberts TPL. Magnetoencephalography and the infant brain. NeuroImage. 2019 Apr 1;189:445–58.

9. Clarke MD, Larson E, Peterson ER, McCloy DR, Bosseler AN, Taulu S. Improving Localization Accuracy of Neural Sources by Pre-processing: Demonstration with Infant MEG Data. Front Neurol. 2022;13:827529.

10. Clarke MD, Bosseler AN, Mizrahi JC, Peterson ER, Larson E, Meltzoff AN, et al. Infant brain imaging using magnetoencephalography: Challenges, solutions, and best practices. Hum Brain Mapp. 2022 Aug 15;43(12):3609–19.

11. Wens V. Exploring the limits of MEG spatial resolution with multipolar expansions. NeuroImage. 2023 Apr 15;270:119953.

12. Feys O, De Tiège X. From cryogenic to on-scalp magnetoencephalography for the evaluation of paediatric epilepsy. Dev Med Child Neurol. 2024 Mar;66(3):298–306.

13. Boto E, Meyer SS, Shah V, Alem O, Knappe S, Kruger P, et al. A new generation of magnetoencephalography: Room temperature measurements using optically-pumped magnetometers. NeuroImage. 2017 Apr 1;149:404–14.

14. Boto E, Holmes N, Leggett J, Roberts G, Shah V, Meyer SS, et al. Moving magnetoencephalography towards real-world applications with a wearable system. Nature. 2018 Mar 29;555(7698):657–61.

15. Brookes MJ, Leggett J, Rea M, Hill RM, Holmes N, Boto E, et al. Magnetoencephalography with optically pumped magnetometers (OPM-MEG): the next generation of functional neuroimaging. Trends Neurosci. 2022 Aug;45(8):621–34.

16. Hill RM, Boto E, Holmes N, Hartley C, Seedat ZA, Leggett J, et al. A tool for functional brain imaging with lifespan compliance. Nat Commun. 2019 Nov 5;10(1):4785.

17. Rier L, Rhodes N, Pakenham D, Boto E, Holmes N, Hill RM, et al. The neurodevelopmental trajectory of beta band oscillations: an OPM-MEG study. eLife. 2024 Feb 15;13.

18. Feys O, Corvilain P, Aeby A, Sculier C, Holmes N, Brookes M, et al. On-Scalp Optically Pumped Magnetometers versus Cryogenic Magnetoencephalography for Diagnostic Evaluation of Epilepsy in School-aged Children. Radiology. 2022 Aug;304(2):429–34.

19. Feys O, Corvilain P, Van Hecke A, Sculier C, Rikir E, Legros B, et al. Recording of Ictal Epileptic Activity Using on-Scalp Magnetoencephalography. Ann Neurol. 2023 Feb;93(2):419–21.

20. Feys O, Ferez M, Corvilain P, Schuind S, Rikir E, Legros B, et al. On-Scalp Magnetoencephalography Based On Optically Pumped Magnetometers Can Detect Mesial Temporal Lobe Epileptiform Discharges. Ann Neurol. 2024;95(3):620–2.

21. Brookes MJ, Boto E, Rea M, Shah V, Osborne J, Holmes N, et al. Theoretical advantages of a triaxial optically pumped magnetometer magnetoencephalography system. NeuroImage. 2021 Aug 1;236:118025.

22. Boto E, Shah V, Hill RM, Rhodes N, Osborne J, Doyle C, et al. Triaxial detection of the neuromagnetic field using optically-pumped magnetometry: feasibility and application in children. NeuroImage. 2022 May 15;252:119027.

23. Feys O, Corvilain P, Labyt E, Mahmoudzadeh M, Routier L, Sculier C, et al. Tri-axial rubidium and helium optically pumped magnetometers for on-scalp magnetoencephalography recording of interictal epileptiform discharges: a case study. Front Neurosci. 2023;17:1284262.

24. Martynova O, Kirjavainen J, Cheour M. Mismatch negativity and late discriminative negativity in sleeping human newborns. Neurosci Lett. 2003 Apr 10;340(2):75–8.

25. Feys O, Corvilain P, Bertels J, Sculier C, Holmes N, Brookes M, et al. On-scalp magnetoencephalography for the diagnostic evaluation of epilepsy during infancy. Clin Neurophysiol Off J Int Fed Clin Neurophysiol. 2023 Nov;155:29–31.

26. Regan D. Comparison of transient and steady-state methods. Ann N Y Acad Sci. 1982;388:45–71.

27. Kabdebon C, Fló A, de Heering A, Aslin R. The power of rhythms: how steady-state evoked responses reveal early neurocognitive development. NeuroImage. 2022 Jul 1;254:119150.

28. Shibasaki H, Miyazaki M. Event-related potential studies in infants and children. J Clin Neurophysiol Off Publ Am Electroencephalogr Soc. 1992 Jul;9(3):408–18.

29. Wunderlich JL, Cone-Wesson BK, Shepherd R. Maturation of the cortical auditory evoked potential in infants and young children. Hear Res. 2006 Feb;212(1–2):185–202.

30. Fellman V, Huotilainen M. Cortical auditory event-related potentials in newborn infants. Semin Fetal Neonatal Med. 2006 Dec;11(6):452–8.

31. Kushnerenko E, Ceponiene R, Balan P, Fellman V, Näätänen R. Maturation of the auditory change detection response in infants: a longitudinal ERP study. NeuroReport. 2002 Oct 28;13(15):1843.

32. He C, Hotson L, Trainor LJ. Development of infant mismatch responses to auditory pattern changes between 2 and 4 months old. Eur J Neurosci. 2009;29(4):861–7.

33. Bertels J, Bourguignon M, de Heering A, Chetail F, De Tiège X, Cleeremans A, et al. Snakes elicit specific neural responses in the human infant brain. Sci Rep. 2020 May 4;10(1):7443.

34. Nozaradan S, Mouraux A, Cousineau M. Frequency tagging to track the neural processing of contrast in fast, continuous sound sequences. J Neurophysiol. 2017 Jul 1;118(1):243–53.

35. Cirelli LK, Spinelli C, Nozaradan S, Trainor LJ. Measuring Neural Entrainment to Beat and Meter in Infants: Effects of Music Background. Front Neurosci. 2016;10:229.

36. Lenc T, Peter V, Hooper C, Keller PE, Burnham D, Nozaradan S. Infants show enhanced neural responses to musical meter frequencies beyond low-level features. Dev Sci. 2023 Sep;26(5):e13353.

37. Edalati M, Wallois F, Safaie J, Ghostine G, Kongolo G, Trainor LJ, et al. Rhythm in the Premature Neonate Brain: Very Early Processing of Auditory Beat and Meter. J Neurosci Off J Soc Neurosci. 2023 Apr 12;43(15):2794–802.

38. Näätänen R, Paavilainen P, Rinne T, Alho K. The mismatch negativity (MMN) in basic research of central auditory processing: a review. Clin Neurophysiol Off J Int Fed Clin Neurophysiol. 2007 Dec;118(12):2544–90.

39. de Lange P, Boto E, Holmes N, Hill RM, Bowtell R, Wens V, et al. Measuring the cortical tracking of speech with optically-pumped magnetometers. NeuroImage. 2021 Jun;233:117969.

40. He C, Hotson L, Trainor LJ. Mismatch responses to pitch changes in early infancy. J Cogn Neurosci. 2007 May;19(5):878–92.

41. Lew S, Sliva DD, Choe M sun, Grant PE, Okada Y, Wolters CH, et al. Effects of sutures and fontanels on MEG and EEG source analysis in a realistic infant head model. NeuroImage. 2013 Aug 1;76:282–93.

42. Aeby A, De Tiège X, Creuzil M, David P, Balériaux D, Van Overmeire B, et al. Language development at 2 years is correlated to brain microstructure in the left superior temporal gyrus at term equivalent age: A diffusion tensor imaging study. NeuroImage. 2013 Sep 1;78:145–51.

43. Wang Q, Zhu GP, Yi L, Cui XX, Wang H, Wei RY, et al. A Review of Functional Near-Infrared Spectroscopy Studies of Motor and Cognitive Function in Preterm Infants. Neurosci Bull. 2019 Nov 12;36(3):321–9.

44. Seymour RA, Alexander N, Mellor S, O'Neill GC, Tierney TM, Barnes GR, et al. Interference suppression techniques for OPM-based MEG: Opportunities and challenges. NeuroImage. 2022 Feb 15;247:118834.

45. Holmes N, Bowtell R, Brookes MJ, Taulu S. An Iterative Implementation of the Signal Space Separation Method for Magnetoencephalography Systems with Low Channel Counts. Sensors. 2023 Jul 20;23(14):6537.

46. Tierney TM, Holmes N, Mellor S, López JD, Roberts G, Hill RM, et al. Optically pumped magnetometers: From quantum origins to multi-channel magnetoencephalography. NeuroImage. 2019 Oct 1;199:598–608.

47. Gutteling TP, Bonnefond M, Clausner T, Daligault S, Romain R, Mitryukovskiy S, et al. A New Generation of OPM for High Dynamic and Large Bandwidth MEG: The 4He OPMs-First Applications in Healthy Volunteers. Sensors. 2023 Mar 3;23(5):2801.

48. QZFM Gen-3 – QuSpin [Internet]. [cited 2024 Mar 25]. Available from: http://quspin.com/products-qzfm/

49. MEGIN-TRIUX-neo-Product-Data-2021.pdf [Internet]. [cited 2024 Mar 25]. Available from: https://megin.com/wp-content/uploads/2022/01/MEGIN-TRIUX-neo-Product-Data-2021.pdf

50. MEGIN-Internal-Helium-Recycler-2021.pdf [Internet]. [cited 2024 Mar 25]. Available from: https://megin.com/wp-content/uploads/2022/01/MEGIN-Internal-Helium-Recycler-2021.pdf

51. "Data Page: Carbon intensity of electricity generation", part of the following publication: Hannah Ritchie, Pablo Rosado and Max Roser (2023) - "Energy". Data adapted from Ember, Energy Institute. Retrieved from https://ourworldindata.org/grapher/carbon-intensity-electricity [online resource].

52. Vigário R, Särelä J, Jousmäki V, Hämäläinen M, Oja E. Independent component approach to the analysis of EEG and MEG recordings. IEEE Trans Biomed Eng. 2000 May;47(5):589–93.

53. Hyvarinen A. Fast ICA for noisy data using Gaussian moments. In: 1999 IEEE International Symposium on Circuits and Systems (ISCAS) [Internet]. 1999 [cited 2024 Mar 25]. p. 57–61 vol.5. Available from: https://ieeexplore.ieee.org/document/777510

54. Oostenveld R, Fries P, Maris E, Schoffelen JM. FieldTrip: Open source software for advanced analysis of MEG, EEG, and invasive electrophysiological data. Comput Intell Neurosci. 2011;2011:156869.

55. Chen L, Wu Z, Hu D, Wang Y, Zhao F, Zhong T, et al. A 4D infant brain volumetric atlas based on the UNC/UMN baby connectome project (BCP) cohort. NeuroImage. 2022 Jun;253:119097.

56. Fonov V, Evans A, McKinstry R, Almli C, Collins D. Unbiased nonlinear average age-appropriate brain templates from birth to adulthood. NeuroImage. 2009 Jul 1;47:S102.

57. Zetter R, Iivanainen J, Parkkonen L. Optical Co-registration of MRI and On-scalp MEG. Sci Rep. 2019 Apr 2;9(1):5490.

58. Gramfort A, Luessi M, Larson E, Engemann DA, Strohmeier D, Brodbeck C, et al. MNE software for processing MEG and EEG data. NeuroImage. 2014 Feb 1;86:446–60.

59. Dale AM, Sereno MI. Improved Localizadon of Cortical Activity by Combining EEG and MEG with MRI Cortical Surface Reconstruction: A Linear Approach. J Cogn Neurosci. 1993;5(2):162–76.

60. Nichols TE, Holmes AP. Nonparametric permutation tests for functional neuroimaging: a primer with examples. Hum Brain Mapp. 2002 Jan;15(1):1–25.

Acknowledgments

Funding:

Fonds Erasme, Convention « Alzheimer » (PC, MF)

Fondation Jaumotte-Demoulin grant (JB)

FRS-FNRS Incentive grant for scientific research F.4503.22 (JB, CC, LF)

FRS-FNRS FRIA grant (OF)

Engineering and Physical Sciences Research Council grant (MB)

Fonds Erasme, Projet de Recherche Clinique
Fonds Erasme, Convention « Les Voies du Savoir 1 & 2 »
FRS-FNRS Research grant J.0043.20F
FRS-FNRS Equipment grant U.N013.21F

Author contributions:

Conceptualization: PC, JB
Methodology: PC
Software: PC
Formal analysis: PC, VW, MB
Investigation: PC, JB, CC, LF, MF
Resources: XDT, OF
Data Curation: PC
Writing—original draft: PC
Writing—review & editing: PC, JB, VW, MB, XDT, CC, MF, OF, LF
Visualization: PC
Supervision: JB, XDT

Competing interests: All the authors declare that they have no competing interests.

Data and materials availability: All data, code, and materials used in the analyses have been archived to an open data publishing platform Zenodo and will be made publicly available upon publication at https://doi.org/10.5281/zenodo.10213856 (dataset) and https://doi.org/10.5281/zenodo.10213974 (code).

Supplementary Material

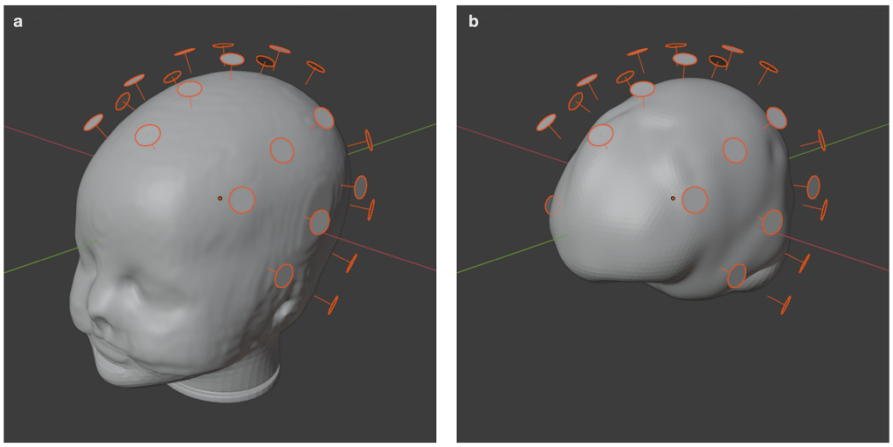

Figure S1. Co-registration procedure. Position and radial axis orientation of the sensors with respect (**a**) to the 3D printed head model, which comes from the infant MNI MRI template and (**b**) to the inner skull surface used for the source reconstruction analysis, which is the adult MNI MRI inner skull surface, shrunk to contain the template BCP brain as snugly as possible.

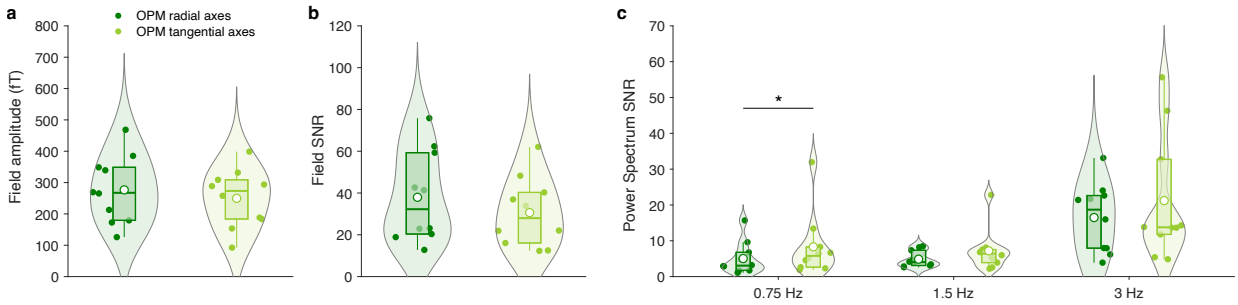

Figure S2. Comparison of the responses recorded by the OPMs on the radial and tangential axes for the 10 participants for whom triaxial sensors were used. (**a**) Amplitude of the evoked responses, (**b**) SNR of the evoked responses and (**c**) power spectrum SNR at the frequencies of interest. The white circles represent the mean of the data. The statistical significance of the comparisons between the axial and tangential axes is indicated above the violin plots. *$p < 0.05$.

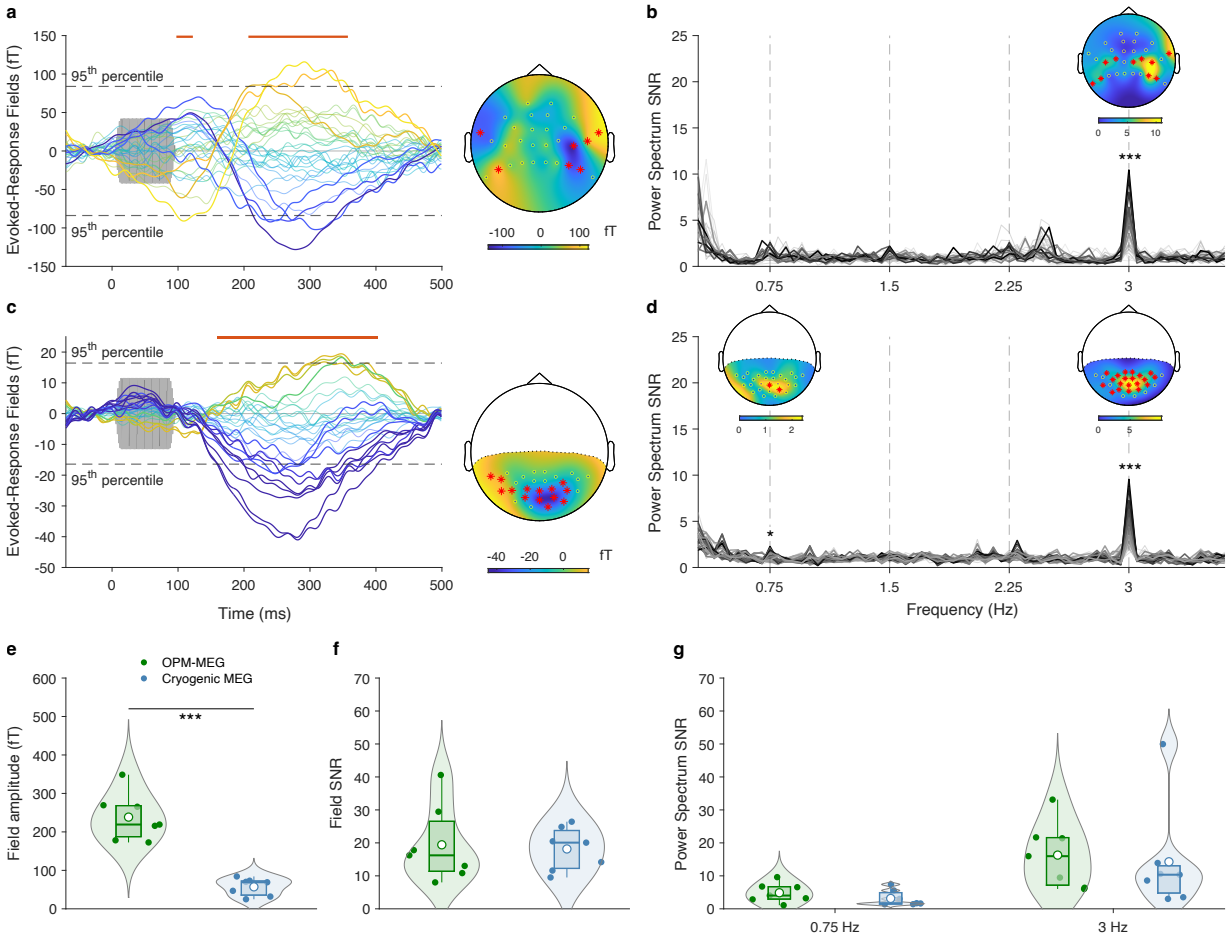

Figure S3. Comparison of the OPM-MEG and cryogenic MEG systems for the 7 participants who underwent the experiments with both modalities. **Left.** Radial magnetic fields evoked in response to single tones measured with (**a**) OPM-MEG and (**c**) cryogenic MEG. The plots are the same as in Fig. 2. Unsurprisingly, given that the infants were lying on their sides in the cryogenic MEG setup, we observed a single dipole in the posterior cryogenic sensors. We also show a comparison of (**e**) the amplitude of the evoked response and (**f**) their SNR. **Right.** Radial magnetic field spectrum SNR for the steady-state response obtained with (**b**) OPM-MEG and (**d**) cryogenic MEG. All is the same as in Fig. 3. (**g**) The power spectrum SNRs are compared at 0.75 Hz and 3 Hz. The white circles represent the mean of the data. The statistical significance of the comparisons between OPM and cryogenic MEG is indicated above the violin plots. ***$p < 0.001$.